On the quantum theory of Brillouin scattering of dielectric layered media

1989 J. Phys.: Condens. Matter 1 3957

(http://iopscience.iop.org/0953-8984/1/25/008)

J. Phys.: Condens. Matter **1** (1989) 3957–3975. Printed in the UK

On the quantum theory of Brillouin scattering of dielectric layered media

A P Mayer†
Department of Physics, University of California, Irvine, CA 92717, USA

Received 1 September 1988

Abstract. The theory of Brillouin scattering of dielectric layered elastic media is formulated in a way that also treats the electromagnetic field quantum mechanically. The general expression for the cross section obtained by this approach is applied to the investigation of shear horizontal modes in the Brillouin spectrum of finite and semi-infinite dielectric superlattices.

1. Introduction

Since the significant achievements concerning the resolution in light scattering experiments [1], Brillouin scattering has become a particularly useful tool for the investigation of long-wavelength acoustic excitations near the surfaces of solid materials as well as in layered structures. The dominant coupling mechanisms between these excitations and the light are the elasto-optic and the ripple effect. The current theories, which have been able to successfully reproduce the experimental data with the elastic, dielectric and elasto-optic constants as parameters, are of a semiclassical nature in that they treat the elastic excitations quantum mechanically, while the electromagnetic field is treated classically. This is sufficient for the interpretation of the Brillouin scattering experiments carried out so far, since they have not been concerned with the quantum properties of the scattered light.

The calculations of the Brillouin spectra in these approaches are largely based on two different methods of solving Maxwell's equations to first order in the elastic displacement field, the Green function method [2] and the matching method [3]. The Green function method requires the knowledge of the Green tensor for the electromagnetic field in the absence of elastic displacements. Once this tensor is established, the Brillouin spectra are obtained by integration over a product involving this Green tensor, the coupling parameters and the displacement–displacement correlation function of the elastic medium. In the matching method, one first calculates the zero-order fields corresponding to a plane wave impinging on the surface of the medium in the absence of elastic deformations. In a second step, the electromagnetic field inside the elastic medium induced by the elastic displacements via the elasto-optic effect is calculated as an inhomogeneous solution of the Maxwell equations to first order in the

† Permanent address: Institut für Theoretische Physik II, Westfälische Wilhelms-Universität, D-4400 Münster, Wilhelm-Klemm-Strasse 10, Federal Republic of Germany.

0953-8984/89/253957 + 19 $02.50

strains. The third step consists in matching a homogeneous solution at the interfaces corrugated by the elastic displacements to fulfil the boundary conditions to first order in these displacements, which yields the scattered field. The appeal of this method consists in its dealing with single waves of the electromagnetic field and directly the normal modes of the displacement field, and one has only to solve linear equations for the amplitudes. The matching of the first-order solutions at the corrugated interfaces is, however, a step that contains some arbitrariness and is not required in the Green function method.

In §§ 2 and 3 the theory of Brillouin scattering of dielectric media is formulated quantum mechanically as the scattering of one-photon states, making use of the dipole approximation from the very beginning and of the normal modes of the electromagnetic field in a layered system. It will be seen that for dielectric layered structures, the quantum mechanical treatment of the electromagnetic field does not lead to any new complications if compared to the quasi-classical approaches. The formulation given here provides, to some extent, a link between the theory of light scattering and the quantum theory for the scattering of atoms and electrons in the distorted-wave Born approximation (DWBA) (for a review, see [4]). The normal modes of the electromagnetic field in the layered structure then correspond to the distorted wave basis set in the latter theories.

Furthermore, this formulation can serve as a starting point for the interpretation of future experiments, in which the quantum statistical properties of the scattered light are analysed to gain information about the corresponding properties of the target system. This may be of interest, for example, if the target degrees of freedom (in our case, the acoustic phonons) obey a non-equilibrium distribution created by the coherent excitation of certain normal modes of that system.

The quantum approach provides an expression for the intensity of the scattered light of the familiar form, namely the square of the modulus of a matrix element multiplied by the spectral function of an elastic mode. As will be demonstrated, the evaluation of this formula appears relatively easy since, like the matching method, it only deals with single modes, while no matching of first-order solutions is required.

Since the hermiticity of the Hamiltonian in the dipole approximation requires the dielectric constants to be real, the result of our quantum formulation is applicable only to those cases where the role of the imaginary parts of the refractive index is negligible.

A brief discussion about the connection between the quantum treatment and the Green function method will be given in § 4. As an illustration, we apply the results of § 2 to the calculation of the Brillouin scattering cross section for finite dielectric superlattices. The elastic vibrations in these structures have been subject to theoretical [5, 6] and experimental investigations, recently also in connection with Brillouin scattering [7–13]. In § 5, the normal modes of the electromagnetic and elastic displacement field are established, which we will use to discuss some general features of the cross section.

In § 6 we give numerical examples for the cross section in the case of crossed polarised backscattering from a finite dielectric superlattice on a reflecting substrate. This scattering geometry is appropriate for the investigation of the elastic modes of shear horizontal polarisation in the layered system. The results presented in § 7 refer to a semi-infinite superlattice in the special situation in which the light enters the superlattice with a finite penetration depth. To our knowledge, a calculation of the Brillouin scattering cross section from semi-infinite superlattices with finite momentum transfer parallel to the surface has not yet been performed. Also, the appearance of the shear horizontal modes in the scattering cross section of finite and infinite superlattices does not seem to have been investigated. In the total reflection geometries chosen for the numerical examples, the application of our approach, which is general for dielectric materials, proves to be particularly easy.

2. The Hamiltonian

To derive the Hamiltonian for the electromagnetic field, one conveniently starts from the Lagrange function in the dipole approximation

$$L = \int \mathrm{d}^3x \, \frac{1}{2}\varepsilon_0 \left(\sum_{\alpha\beta} \varepsilon_{\alpha\beta}(\boldsymbol{x}) \dot{A}_\alpha(\boldsymbol{x}) \dot{A}_\beta(\boldsymbol{x}) - (1/c_0^2)[\mathrm{rot}\, \boldsymbol{A}(\boldsymbol{x})]^2 \right) \tag{2.1}$$

which has to be supplemented by the condition

$$\sum_{\alpha\beta} \nabla_\alpha \{\varepsilon_{\alpha\beta}(\boldsymbol{x}) A_\beta(\boldsymbol{x})\} = 0. \tag{2.2}$$

Here, $\boldsymbol{A}$ denotes the vector potential, c_0 the velocity of the light in a vacuum and $(\varepsilon_{\alpha\beta})$ the dielectric tensor. In writing these equations, we have used a gauge in which the scalar potential vanishes. From now on, the dimensional constant ε_0 will be absorbed in the energy unit. Variation of the Lagrange function with respect to $\dot{\boldsymbol{A}}$ yields the canonical momentum

$$\Pi_\alpha(\boldsymbol{x}) = \sum_\beta \varepsilon_{\alpha\beta}(\boldsymbol{x}) \dot{A}_\beta(\boldsymbol{x}) \tag{2.3}$$

and after a Legendre transformation, we obtain the Hamiltonian

$$H = \int \mathrm{d}^3x \, \frac{1}{2} \left(\sum_{\alpha\beta} [\varepsilon^{-1}(x)]_{\alpha\beta} \Pi_\alpha(\boldsymbol{x}) \Pi_\beta(\boldsymbol{x}) + (1/c_0^2)[\mathrm{rot}\, \boldsymbol{A}(\boldsymbol{x})]^2 \right) + H_\mathrm{p} \tag{2.4}$$

where the Hamiltonian of the pure phonon system, H_p, has been added. We now decompose this Hamiltonian in an unperturbed part

$$H_0 = \int \mathrm{d}^3x \, \tfrac{1}{2} \{\varepsilon_{(0)}^{-1}(z) \boldsymbol{\Pi}(\boldsymbol{x}) \cdot \boldsymbol{\Pi}(\boldsymbol{x}) + (1/c_0^2)[\mathrm{rot}\, \boldsymbol{A}(\boldsymbol{x})]^2\} + H_\mathrm{p} \tag{2.5}$$

and a part to which perturbation theory will be applied,

$$\begin{aligned} H' = & -\frac{1}{2} \int \mathrm{d}^3x \, \varepsilon_{(0)}^{-2}(z) \sum_{\alpha\beta} \delta\varepsilon_{\alpha\beta}(\boldsymbol{x}) \Pi_\alpha(\boldsymbol{x}) \Pi_\beta(\boldsymbol{x}) \\ & + \frac{1}{2} \int \mathrm{d}^2R \sum_j \left(\int_{z_j}^{z_j + u_z(\boldsymbol{R}, z_j)} \mathrm{d}z \, \varepsilon_{j-1}^{-1} \sum_\alpha \Pi_\alpha^2(\boldsymbol{x}) \right. \\ & \left. + \int_{z_j + u_z(\boldsymbol{R}, z_j)}^{z_j} \mathrm{d}z \, \varepsilon_j^{-1} \sum_\alpha \Pi_\alpha^2(\boldsymbol{x}) \right). \end{aligned} \tag{2.6}$$

The dielectric tensor has been split into a part of purely electronic origin $\varepsilon_{(0)}$, which for simplicity is taken to be isotropic and homogeneous in each layer,

$$\varepsilon_{(0)}(z) = \varepsilon_j \qquad \text{for } z_j < z < z_{j+1} \tag{2.7}$$

and a contribution $(\delta\varepsilon_{\alpha\beta})$, which represents the coupling of the light to the elastic deformations via the elasto-optic effect and which is itself an operator in the Hilbert space of the elastic degrees of freedom.

$$\delta\varepsilon_{\alpha\beta}(\boldsymbol{x}) = \varepsilon_j^2 \sum_{\mu\nu} p_{\alpha\beta\mu\nu}^{(j)} \tfrac{1}{2} (\nabla_\nu u_\mu(\boldsymbol{x}) + \nabla_\mu u_\nu(\boldsymbol{x})) \qquad \text{for } z_j < z < z_{j+1} \tag{2.8}$$

where $p_{\alpha\beta\mu\nu}$ are the Pockels coefficients and $\boldsymbol{u}(\boldsymbol{x})$ is the displacement field. The second

term in (2.6) represents the ripple effect. We have chosen the z axis to be normal to the layers, and z_j marks the position of the undeformed interface between the $(j-1)$th and the jth layers.

In order to diagonalise the electromagnetic part of the unperturbed Hamiltonian H_0, we perform a canonical transformation to normal coordinates $Q(\lambda)$ and conjugate momenta $P(\lambda)$. They are associated with a set of basis functions $\boldsymbol{c}(\boldsymbol{x}|\lambda)$ orthonormal with respect to the scalar product

$$\langle f, g\rangle = \int \mathrm{d}^3x\, \varepsilon_{(0)}(z) f^*(\boldsymbol{x}) g(\boldsymbol{x}) \tag{2.9}$$

where $\boldsymbol{f}$ and $\boldsymbol{g}$ are two vectors of the Hilbert space under consideration†. The basis set should contain the incoming states in the spirit of the DWBA. The transformation then reads

$$\boldsymbol{A}(\boldsymbol{x}) = \sum_{\lambda} Q(\lambda)\boldsymbol{c}(\boldsymbol{x}|\lambda) \tag{2.10}$$

$$\boldsymbol{\Pi}(\boldsymbol{x}) = \sum_{\lambda} P(\lambda)\boldsymbol{c}(\boldsymbol{x}|\lambda)\varepsilon_{(0)}(z). \tag{2.11}$$

The functions are now chosen to be the eigenvectors of the operator $\varepsilon_{(0)}^{-1}(z)\Delta$, satisfying the transversality condition in each layer and the conditions of the continuity of $\boldsymbol{A}_{\parallel}$, $\varepsilon_{(0)}\boldsymbol{A}_{\perp}$ and $\mathrm{rot}\,\boldsymbol{A}$ at each interface, i.e., they are the solutions of the field equations resulting from the Lagrange function (2.1) for a given frequency. In addition, we require periodic boundary conditions in the x–y plane. The index λ, which labels these eigenmodes, can then be chosen as

$$\lambda \simeq (\boldsymbol{k}, s, \tau) \tag{2.12}$$

where $\boldsymbol{k}$ is the wavevector in vacuum, s denotes the polarisation, and τ is an additional index that will be specified in § 5. It is then an easy matter to show, that H_0 takes the form of the Hamiltonian for a set of decoupled oscillators with frequencies

$$\omega_\lambda = kc_0. \tag{2.13}$$

3. The scattered intensity

The following derivation of the power spectrum of the scattered light largely follows the derivation of the cross section for atom and electron scattering of solid surfaces in the DWBA [4]. From general quantum mechanical scattering theory [14], the scattered part of the outgoing wavefunction is given by

$$|\psi_{\mathrm{out}}(t)\rangle_{\mathrm{s}} = -\frac{2\pi\mathrm{i}}{\hbar}\sum_{\nu'\lambda'} |\lambda'\nu'\rangle\, \mathrm{e}^{\mathrm{i}(\omega_{\lambda'}+\omega_{\nu'})t}\delta(\omega_{\lambda'}+\omega_{\nu'}-\omega_{\lambda_0}-\omega_{\nu})$$
$$\times \langle\lambda\nu'|T(\omega_{\lambda_0}+\omega_{\nu}+\mathrm{i}\varepsilon)|\lambda_0\nu\rangle \tag{3.1}$$

in terms of the T-operator. The symbol $|\lambda\nu\rangle$ denotes the product of an eigenstate of the pure phonon Hamiltonian with quantum numbers ν and a photon state characterised by λ. In the following, only one-photon scattering is considered, and for sake of simplicity,

† One can also work with the usual scalar product after transition to functions $\boldsymbol{c}'(\boldsymbol{x}|\lambda) = \sqrt{\varepsilon_{(0)}(z)}\,\boldsymbol{c}(\boldsymbol{x}|\lambda)$. We shall pursue this way for the elastic modes, where the same problem arises with the mass densities.

we may confine ourselves to one-phonon-states for the incoming and outgoing states. A generalisation to superpositions of states with different photon numbers, such as coherent states, is possible in principle. In view of the first Born approximation that we will employ later on, we write

$$T(\omega_{\lambda_0} + \omega_\nu + i\varepsilon)|\lambda_0 \nu\rangle = H'|\lambda_0 \nu +\rangle \tag{3.2}$$

which is still exact. Here, $|\lambda_0 \nu +\rangle$ is the eigenstate of $H_0 + H'$, into which $|\lambda_0 \nu\rangle$ develops if H' is switched on adiabatically.

The power spectrum of the scattered light may be calculated using the formula

$$I_{\alpha\beta}(\omega) = \left\langle \int \mathrm{d}t' \, \mathrm{e}^{-i\omega t'} {}_s\langle \psi_{\text{out}} | \dot{A}_\alpha(\boldsymbol{x}, t) \dot{A}_\beta(\boldsymbol{x}, t+t') | \psi_{\text{out}} \rangle_s \right\rangle \tag{3.3}$$

where $\boldsymbol{x}$ is the position of the detector. The time dependence of the field operators in (3.3) is governed by the unperturbed Hamiltonian. The additional angular brackets in this equation mean that the sum over the final phonon states and the average (in our case the thermal average) of the initial phonon states have to be performed. After insertion of (2.10) and (3.1) into (3.3), and the introduction of phonon creation and annihilation operators in the standard way, we obtain

$$\begin{aligned} I_{\alpha\beta}(\omega) = \frac{4\pi^3}{\hbar} \sum_{\lambda'\lambda''\nu\nu'} & \langle +\nu\lambda_0 | H' | \lambda'\nu' \rangle \langle \nu'\lambda'' | H' | \lambda_0 \nu + \rangle \rho_\nu [\omega_{\lambda'} \omega_{\lambda''}]^{1/2} \\ & \times c_\alpha(\boldsymbol{x}|\lambda'') c_\beta(\boldsymbol{x}|\bar{\lambda}') \, \mathrm{e}^{i(\omega_{\lambda'} - \omega_{\lambda''})t} \delta(\omega_{\lambda'} + \omega_{\nu'} - \omega_{\lambda_0} - \omega_\nu) \\ & \times \delta(\omega_{\lambda''} + \omega_{\nu'} - \omega_{\lambda_0} - \omega_\nu) \delta(\omega - \omega_{\lambda'}) \end{aligned} \tag{3.4}$$

where the term resulting from the commutator of the two field operators in (3.3) has been dropped. ρ_ν is the thermal weight of the phonon state with quantum numbers ν. The perturbation Hamiltonian H' may now be expanded with respect to phonon normal coordinates,

$$H' = \sum_\mu V(\mu) B(\mu). \tag{3.5}$$

The index μ stands for the part $\boldsymbol{Q}$ of the phonon wavevector parallel to the x–y plane and a further index J, which labels the different modes with the same $\boldsymbol{Q}$. The coordinates B are connected with the displacement field via

$$\boldsymbol{u}(\boldsymbol{x}) = \frac{1}{L} \sum_{\boldsymbol{Q}J} \left[\frac{\hbar}{2\omega_{\boldsymbol{Q}J} \rho(z)} \right]^{1/2} \mathrm{e}^{i\boldsymbol{Q}\cdot\boldsymbol{x}_\parallel} \boldsymbol{w}(z|\boldsymbol{Q}J) B(\boldsymbol{Q}J). \tag{3.6}$$

Throughout this paper, we assume periodic boundary conditions in the x–y plane with length of periodicity L. After replacing $\omega_{\lambda 0} + \omega_\nu$ by $\omega_{\lambda'} + \omega_{\nu'}$ in the argument of the second δ-function in (3.4) and approximating $|\lambda\nu +\rangle$ by a product state, where the phonon part is given by the corresponding eigenstate of H_p, the sums over ν and ν' may be performed by introducing the spectral density function S:

$$2\pi \sum_{\nu\nu'} \rho_\nu \delta(\omega_{\nu'} - \omega_\nu + \Omega) \langle \nu | B(\mu) | \nu' \rangle \langle \nu' | B(\mu') | \nu \rangle = \delta_{\bar{\mu}\mu'} S_\mu(\Omega). \tag{3.7}$$

This leads to the result

$$\begin{aligned} I_{\alpha\beta}(\omega) = \frac{2\pi^2}{\hbar} \omega \sum_{\lambda'\lambda''} & c_\alpha(\boldsymbol{x}|\lambda'') c_\beta(\boldsymbol{x}|\bar{\lambda}') \delta(\omega - \omega_{\lambda'}) \delta(\omega_{\lambda'} - \omega_{\lambda''}) \\ & \times \sum_\mu \langle +\lambda_0 | V(\mu) | \lambda' \rangle \langle \lambda'' | V(\bar{\mu}) | \lambda_0 + \rangle S_\mu(\omega_{\lambda'} - \omega_{\lambda_0}) \end{aligned} \tag{3.8}$$

which bears the familiar features of the scattered intensity of a projectile at an arbitrary system in the first Born approximation in that it contains the spectral density of the degrees of freedom probed, twice multiplied with a matrix element of the coupling between these degrees of freedom and the projectile. A further simplification can be achieved by making use of the wavevector conservation within the x–y plane in the matrix elements, which is satisfied for the systems we have in view. On decomposing

$$c_\alpha(\boldsymbol{x}|\boldsymbol{k}s\tau) = (1/L)^{\mathrm{i}\boldsymbol{K}\cdot\boldsymbol{x}}\tilde{c}_\alpha(\boldsymbol{x}|\boldsymbol{k}s\tau) \tag{3.9}$$

we arrive at our final result

$$I^{(ss_0)}(\omega) = \frac{2\pi^2\omega}{\hbar L^2 c_0^4}\sum_{QJ}\left(\frac{\omega}{k_z}\right)^2 |M(\boldsymbol{k}\boldsymbol{k}_0|ss_0|J)|^2 S_{QJ}(\omega - \omega_{k_0}) \tag{3.10}$$

where

$$\boldsymbol{k}_0 = (\boldsymbol{K}_0, k_{0z}) \qquad \boldsymbol{k} = (\boldsymbol{K}, k_z) \qquad k_z = \left[\left(\frac{\omega}{c_0}\right)^2 - K^2\right]^{1/2}. \tag{3.11}$$

For harmonic phonons, the spectral density function S is of the form

$$S_{QJ}(\Omega) = 2\pi\{(n_{QJ}+1)\delta(\Omega - \omega_{QJ}) + n_{QJ}\delta(\Omega + \omega_{QJ})\} \tag{3.12}$$

where n_{QJ} are the thermal quantum numbers. In order to obtain the scattering cross section, the sum over $\boldsymbol{Q}$ in (3.10) has to be replaced by kinematic factors [3, 15]

$$\frac{1}{L^2}\sum_{\boldsymbol{Q}} \leftrightarrow \text{const.}\,\frac{\omega_0\cos^2\theta_\mathrm{f}}{\hbar\cos\theta_\mathrm{i}}. \tag{3.13}$$

The factor ω_0 instead of ω_0^2 in (3.13) results from the fact that the incoming intensity for the one-phonon state is proportional to ω_0.

We now discuss the functions M. They consist of a contribution due to the elasto-optic and a contribution due to the ripple effect. The first is given by

$$M^{(\mathrm{e})}(\boldsymbol{k}\boldsymbol{k}_0|ss_0|J) = -\frac{\hbar}{4}\omega\sum_\tau D(\boldsymbol{k}s\tau)\int_{-\infty}^{0}\mathrm{d}z\sum_{\alpha\beta}\delta\varepsilon_{\alpha\beta}(z|\boldsymbol{K}-\boldsymbol{K}_0J)$$
$$\times\,\tilde{c}^*_\alpha(z|\boldsymbol{k}s\tau)\tilde{c}_\beta(z|\boldsymbol{k}_0s_0\tau_0) \tag{3.14}$$

where

$$\delta\varepsilon_{\alpha\beta}(z|\boldsymbol{Q}J) = -\varepsilon_j^2\sum_{\mu\nu}p^{(j)}_{\alpha\beta\mu\nu}\left(\frac{\hbar}{2\omega_{QJ}\rho(z)}\right)^{1/2}$$
$$\times\,[\mathrm{i}Q_\nu(1-\delta_{\nu z}) + \nabla_z\delta_{\nu z}]w_\mu(z|\boldsymbol{Q}J) \tag{3.15}$$

while the latter is of the form

$$M^{(\mathrm{r})}(\boldsymbol{k}\boldsymbol{k}_0|ss_0|J) = \frac{\hbar}{4}\omega\sum_\tau D(\boldsymbol{k}s\tau)\left(\frac{\hbar}{2\omega_{QJ}\rho_j}\right)^{1/2}\sum_j w_z(z_j|\boldsymbol{Q}J)(\varepsilon_j - \varepsilon_{j-1})$$
$$\times\sum_\alpha \tilde{c}^*_\alpha(z_{j\mp}|\boldsymbol{k}s\tau)\tilde{c}_\alpha(z_{j\pm}|\boldsymbol{k}_0s_0\tau_0). \tag{3.16}$$

$D(\boldsymbol{k}s\tau)$ is the amplitude of the plane-wave component of the function $\boldsymbol{c}(\boldsymbol{x}|\boldsymbol{k}s\tau)$ which radiates into the vacuum. To obtain (3.16), one has to argue in the same way as in [2]

for the Green function method, namely that the field associated with the state $|\lambda+\rangle$ has its discontinuities at the corrugated interfaces, while the states $|\lambda\rangle$ are associated with the functions $\boldsymbol{c}$, which are discontinuous at the non-corrugated interfaces. Furthermore, we have made use of the relation

$$\tilde{c}_\alpha^*(z_{j\pm}|\boldsymbol{k}s\tau)\tilde{c}_\alpha(z_\mp|\boldsymbol{k}_0 s_0\tau_0) = \tilde{c}_\alpha^*(z_{j\mp}|\boldsymbol{k}s\tau)\tilde{c}_\alpha(z_{j\pm}|\boldsymbol{k}_0 s_0\tau_0) \tag{3.17}$$

which follows from the boundary conditions fulfilled by the functions $\boldsymbol{c}$. The symbols z_{j+} and z_{j-} mean that the jth interface is approached from above or below. Either the upper or the lower set of signs in (3.16) may be chosen.

4. Connection with the Green function approach

The result (3.10), together with (3.14) and (3.16), may also be obtained in a quasi-classical approach using the Green tensor $[G_{\alpha\beta}(\boldsymbol{x}, \boldsymbol{x}', \Delta t)]$ of the electromagnetic field. This is briefly outlined in this section. A shorthand notation is used, in which matrix multiplication includes spatial integration.

In the Green function method, the actual electromagnetic field $\boldsymbol{A}(t)$ is calculated from the equation

$$\boldsymbol{A}(t) = \boldsymbol{A}^{(\mathrm{i})}(t) + \int \mathrm{d}t' \mathbf{G}_\mathrm{r}(t-t')\mathbf{V}(t')\boldsymbol{A}^{(\mathrm{i})}(t'). \tag{4.1}$$

Here, $\mathbf{G}_\mathrm{r}$ is the retarded Green tensor, $\boldsymbol{A}^{(\mathrm{i})}$ is the solution of the field equations in the absence of elastic deformations associated with the incoming beam, i.e.,

$$\boldsymbol{A}^{(\mathrm{i})}(\boldsymbol{x}, t) \sim \boldsymbol{c}(\boldsymbol{x}|\lambda_0) \tag{4.2}$$

and $\mathbf{V}$ contains the coupling via the elasto-optic and ripple effect. The retarded Green tensor may now be written in terms of the normal modes of the field as follows:

$$G_{\alpha\beta}(\boldsymbol{x}, \boldsymbol{x}, \Delta t) = -c_0^2 \int_{-\infty}^{\infty} \frac{\mathrm{d}\omega}{2\pi} \sum_\lambda \frac{c_\alpha(\boldsymbol{x}|\lambda)c_\beta^*(\boldsymbol{x}'|\lambda)}{(\omega + \mathrm{i}\varepsilon)^2 - \omega_\lambda^2} \mathrm{e}^{-\mathrm{i}\omega\Delta t}. \tag{4.3}$$

Since the set of functions in the representation (4.3) has to be complete, those optical modes that are localised in the layered structure also have to be included. These, however, do not contribute to the scattering in lowest order perturbation theory. $\boldsymbol{A}(t)$ in (4.1) can now be regarded as the field, into which the field configuration $\boldsymbol{A}^{(\mathrm{i})}$ develops, if the perturbation is switched on adiabatically at $t \to -\infty$. In the spirit of **S**-matrix theory, the scattered field $\boldsymbol{A}^{(\mathrm{s})}$ is obtained from the actual field by switching the perturbation off adiabatically employing the relation

$$\boldsymbol{A}(t) = \boldsymbol{A}^{(\mathrm{s})}(t) + \int \mathrm{d}t'\, \mathbf{G}_\mathrm{a}(t-t')\mathbf{V}(t')\boldsymbol{A}^{(\mathrm{s})}(t') \tag{4.4}$$

where $\mathbf{G}_\mathrm{a}$ is the advanced Green tensor, which is given by the RHS of (4.3) with, however, the sign in front of $\mathrm{i}\varepsilon$ reversed. Equating the RHS of (4.1) and (4.4) and solving for $\boldsymbol{A}^{(\mathrm{s})}$ yields to lowest order in the perturbation

$$\boldsymbol{A}^{(\mathrm{s})}(t) = \boldsymbol{A}^{(\mathrm{i})}(t) + \int \mathrm{d}t' \{\mathbf{G}_\mathrm{r}(t-t') - \mathbf{G}_\mathrm{a}(t-t')\}\mathbf{V}(t')\boldsymbol{A}^{(\mathrm{i})}(t'). \tag{4.5}$$

Using the spectral representation (4.3) of the Green functions one may now proceed as

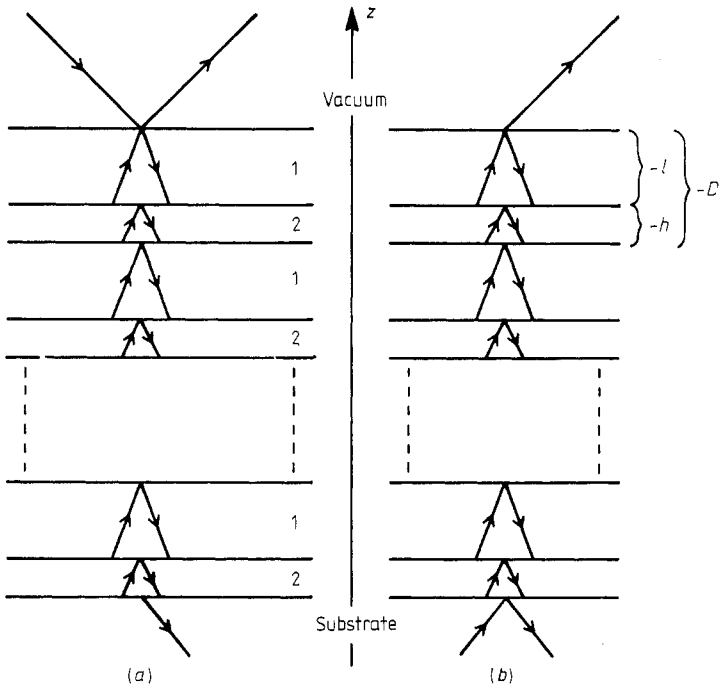

Figure 1. Schematic representation of the normal modes of the electromagnetic field.

in § 3 to calculate the power spectrum of the scattered field. The difference between the retarded and the advanced Green functions in (4.5) generates the first two δ-functions in (3.4), and no principal values appear.

5. Normal modes of the electromagnetic and displacement field

As an example, we now discuss the situation of a finite dielectric superlattice on a substrate, which will be assumed to be also dielectric in the first part and totally reflecting in the second part. The functions $c(x|\lambda)$ can be constructed by superposing two plane waves in each medium and matching their amplitudes via the boundary conditions at the interfaces.

$$\begin{aligned}
\tilde{c}(z|\lambda) &= A_{v+}(\lambda)\,e^{iq_0 z} + A_{v-}(\lambda)\,e^{-q_0 z} && \text{for } z > 0 \\
&= A_{1+}^{(n)}(\lambda)\,e^{iq_1(z-nD)} + A_{1-}^{(n)}(\lambda)\,e^{-iq_1(z-nD)} && \text{for } nD + l < z < nD \\
&= A_{2+}^{(n)}(\lambda)\,e^{iq_2(z-nD)} + A_{2-}^{(n)}(\lambda)\,e^{-iq_2(z-nD)} && \text{for } (n+1)D < z < nD + l \\
&= A_{s+}(\lambda)\,e^{iq_s(z-ND)} + A_{s-}(\lambda)\,e^{-iq_s(z-ND)} && \text{for } z < ND
\end{aligned} \tag{5.1}$$

and

$$k_z = q_0 \qquad k^2 = K^2 + q_0^2 = \varepsilon_1^{-1}(K^2 + q_1^2) = \varepsilon_2^{-1}(K^2 + q_2^2) = \varepsilon_s^{-1}(K^2 + q_s^2). \tag{5.2}$$

In the first case, we distinguish two types of modes ($\tau = a, b$), shown schematically in figure 1. The modes of the first type, which contain the incoming states, do not contain

a component which radiates out of the substrate, while the second type has only one component in the vacuum. It is most convenient to refer the amplitudes via transfer matrices [16] to a reference amplitude, the value of which is determined by the normalisation. Only the vacuum and substrate parts enter the normalisation integrals (analogous to the normalisation of bulk elastic modes in layered media [17]), and it can easily be shown that the above modes are normalised, if $|A_{v-}|$ for the modes of type a and $|A_{s+}|$ for the modes of type b are chosen to be $[2\pi]^{-1/2}$. In the case of a totally reflecting substrate, the modes of type b are absent, and $|A_{v+}|$ and $|A_{v-}|$ are equal. Without loss of generality, we assume $\boldsymbol{K}$ parallel to the x-axis. For the TE-polarised modes, we decompose

$$\boldsymbol{A}_{j\pm} = \hat{y}A_{j\pm} \tag{5.3}$$

and for the TM modes

$$\boldsymbol{A}_{j\pm} = [1 + q_0^2/k^2]^{-1/2}[\hat{z} \mp (q_i/K)\hat{x}]A_{j\pm}. \tag{5.4}$$

One has then only to deal with two-component vectors (A_{j+}, A_{j-}) and 2×2 matrices:

$$\begin{pmatrix} A_{1+}^{(n)} \\ A_{1-}^{(n)} \end{pmatrix} = \mathbf{T} \begin{pmatrix} A_{1+}^{(n+1)} \\ A_{1-}^{(n+1)} \end{pmatrix} \tag{5.5}$$

$$\begin{pmatrix} A_{1+}^{(n)} \\ A_{1-}^{(n)} \end{pmatrix} = \mathbf{M} \begin{pmatrix} A_{2+}^{(n)} \\ A_{2-}^{(n)} \end{pmatrix} \tag{5.6}$$

The transfer matrices $\mathbf{T}$ and matrices $\mathbf{M}$ are specified in the Appendix.

The normal modes of the displacement field are determined in a similar way. Here, however, the z-component of the wavevector may be complex, and in the most general case, up to six instead of only two components may occur in the decomposition of $w(z|QJ)$ analogous to (5.1). In elastically isotropic materials, the sagittal modes can be separated from the shear horizontals, and the amplitude vectors of the first consists of four components, while the one for the latter has only two. Like their optic analogues, the elastic transfer matrices have the property that each eigenvalue occurs together with its inverse. The elastic modes of the system under consideration can be divided into three categories.

(1) Localised modes of the superlattice, which correspond to an eigenvalue of the transfer matrix, the modulus of which is not unity and decay both in the superlattice and in the substrate.

(2) Band modes of the superlattice, which correspond to eigenvalues of the transfer matrix, which are phase factors. They propagate plane-wave-like in the superlattice and decay in the substrate. For sufficiently large numbers of layers, they form continuous bands.

(3) Bulk modes of the substrate, which may show resonances in the superlattice.

From these properties of the optic and acoustic modes, some general conclusions concerning the Brillouin cross section may be drawn. The function M in the expression for the scattered intensity (3.10) can be cast into the following form:

$$M(\boldsymbol{k}\boldsymbol{k}_0|ss_0|J) = E(\boldsymbol{k}\boldsymbol{k}_0|ss_0|JN) + \sum_{\sigma_1\sigma_2\sigma_3=\pm} \sum_j F_{\sigma_1\sigma_2\sigma_3 j}(\boldsymbol{k}\boldsymbol{k}_0|ss_0|JN)$$
$$\times \frac{[\lambda_j^{\sigma_1}(\boldsymbol{K}-\boldsymbol{K}_0J)\lambda^{*\sigma_2}(\boldsymbol{k}s)\lambda^{\sigma_3}(\boldsymbol{K}_0s_0)]^N - 1}{1-\lambda_j^{-\sigma_1}(\boldsymbol{K}-\boldsymbol{K}_0J)\lambda^{*-\sigma_2}(\boldsymbol{k}s)\lambda^{-\sigma_3}(\boldsymbol{k}_0s_0)} \tag{5.7}$$

because after diagonalising the three transfer matrices involved, the integral in (3.14) can be converted into an integral over the 'unit cell' of the superlattice and a sum over all units, which, like the sum in (3.16), is a geometrical series in the product of the eigenvalues of the transfer matrices. The coefficients F also contain the reference amplitudes, which in general depend on N. The function E takes account of the elasto-optic contribution from the substrate and the ripple contribution from the vacuum interface and partly the substrate interface. If all three eigenvalues occurring in (5.7) are phase factors, we may express them as

$$\lambda_j(\boldsymbol{QJ}) = \mathrm{e}^{\mathrm{i}\zeta D} \qquad \lambda(\boldsymbol{ks}) = \mathrm{e}^{\mathrm{i}\xi D} \qquad \lambda(\boldsymbol{k}_0 s_0) = \mathrm{e}^{\mathrm{i}\xi_0 D} \tag{5.8}$$

where $\zeta(\boldsymbol{QJ})$, $\xi(\boldsymbol{ks})$ and $\xi_0(\boldsymbol{k}_0 s_0)$ are the effective wavenumbers of the acoustic mode and the light in the layered structure. The ratio in (5.7) then takes the form

$$\frac{\exp[\mathrm{i}ND(\sigma_1\zeta - \sigma_2\xi + \sigma_3\xi_0] - 1}{1 - \exp[-\mathrm{i}(\sigma_1\zeta - \sigma_2\xi + \sigma_3\xi_0)]}. \tag{5.9}$$

The modulus square of this expression, which will occur in the formula for the scattered intensity, approaches for large N a δ-function. This result expresses the conservation of the effective wavevectors *modulo* a reciprocal wavevector of the superlattice and gives rise to resonances in the spectrum. This has been found by Babiker *et al* [8] and by He *et al* [12] in the case of longitudinal phonons and normal incidence of the light. It should be noted, that unlike in the single interface case, also the ripple scattering contributes to this quasi-momentum conservation because of the periodicity of the interfaces. The ratio

$$\frac{2|\varepsilon_2 - \varepsilon_1|}{|\overline{\varepsilon^2 p_{13}}|D|\omega - \omega_0|/\bar{c}_l} \tag{5.10}$$

may be regarded as a very rough estimate for the relative importance of the ripple effect in comparison to the elasto-optic effect for the peak intensities of the longitudinal acoustic band modes for the case of normal incidence. Here, $\overline{\varepsilon^2 p_{13}}$ is the average of $\varepsilon_j^2 p_{13}^{(j)}$, and $\bar{c}_l$ the average longitudinal sound velocity. If the dielectric constants are sufficiently different, the ripple contribution can become significant and due to its interference with the elasto-optic contribution increase or decrease the peak intensities.

The behaviour of the cross section is totally different, if one of the three eigenvalues λ in (5.7) is not a phase factor. This may occur in the following cases.

(1) The acoustic mode is a localised mode in the superlattice. In this case, the spectrum shows a discrete δ-peak from the spectral density function S in (3.10).

(2) The acoustic mode corresponds to a bulk phonon of the substrate with a displacement field in the superlattice which is largely localised at the vacuum and substrate interface. Such modes may show resonances in the continuous part of the Brillouin spectrum, which are however of a different origin, e.g. due to an enhancement of E in (5.7) because of possible high amplitudes at the substrate and/or vacuum interfaces.

(3) The incident or scattered light corresponds to a forbidden optical band of the superlattice. We shall address this peculiar situation at the end of § 6.

6. Shear horizontal modes in a dielectric superlattice on a metallic substrate

In this section, a numerical example is given for a situation, to which the application of the present approach is particularly easy, namely the investigation of shear horizontal

acoustic phonons in a finite dielectric superlattice on a metal substrate, which we approximate to be totally reflecting for the light. By choosing a geometry in which $\boldsymbol{K}$ and $\boldsymbol{K}_0$ are parallel, the incident light is TE-polarised and only the TM component of the scattered light is analysed, we make sure that only the shear horizontal modes will be seen in the spectrum. Since these modes do not produce interface ripples, only the elasto-optic coupling is effective and the function E in (5.7) vanishes. Explicit expressions for F are given in the Appendix.

We now address the calculation of the elastic modes. Shear horizontal modes in superlattices have been discussed in detail by Camley *et al* [5]. We will make use of their results for the semi-infinite superlattice and extend them to account for the presence of the substrate. We assume the films as well as the substrate to be elastically isotropic. The parameters entering the calculation are then the bulk shear velocities c_j and the densities ρ_j of the three materials ($j = 1, 2, \mathrm{s}$). We then define

$$\alpha_j = [Q^2 - (\Omega/c_j)^2]^{1/2} \tag{6.1}$$

$$\beta_j = \alpha_j \rho_j c_j^2 \tag{6.2}$$

for a given wavevector $\boldsymbol{Q}$ parallel in the x–y plane. Below the bulk threshold of the substrate, the mode frequencies Ω_{Qj} are the solutions of the equation

$$\begin{pmatrix} 1 \\ -1 \end{pmatrix} \mathbf{R} \begin{pmatrix} \lambda^N & 0 \\ 0 & \lambda^{-N} \end{pmatrix} \mathbf{R}^{-1} \begin{pmatrix} \beta_1 + \beta_\mathrm{s} \\ \beta_1 - \beta_\mathrm{s} \end{pmatrix} = 0. \tag{6.3}$$

Here, λ and λ^{-1} are the eigenvalues of the elastic transfer matrix given in the Appendix,

$$\lambda = t \pm [t^2 - 1]^{1/2} \tag{6.4}$$

with

$$t = \cosh(\alpha_1 l)\cosh(\alpha_2 h) + \frac{1}{2}\left(\frac{\beta_1}{\beta_2} + \frac{\beta_2}{\beta_1}\right)\sinh(\alpha_1 l)\sinh(\alpha_2 h) \tag{6.5}$$

and the matrix $\mathbf{R}$ contains as columns the two eigenvectors. The role of condition (6.3) can be regarded as discretising the band modes and shifting the position of (and eventually excluding) the localised modes of the semi-infinite superlattice. With increasing N, the bands will be filled by modes with $|\lambda| = 1$. For $|\lambda| > 1$, we may for large N neglect the term with λ^{-N}, and the LHS of (6.3) factorises into two terms. The zeros of the first correspond to the localised modes of a semi-infinite superlattice discussed by Camley *et al* [5]. The second term equated to zero provides the condition for the existence of modes localised at the substrate interface. It can be cast into the form

$$\left\{\frac{\beta_1\beta_\mathrm{s}}{\beta_1+\beta_\mathrm{s}}\left(\frac{\beta_1}{\beta_2} - \frac{\beta_2}{\beta_1}\right)\mathrm{e}^{-\alpha_1 l}\cosh^{-1}(\alpha_1 l) - \beta_1\frac{\beta_\mathrm{s}}{\beta_2} + \beta_2\right\}\tanh(\alpha_2 h)$$
$$+ (\beta_1 - \beta_\mathrm{s})\tanh(\alpha_1 l) = 0. \tag{6.6}$$

These modes decay into the substrate with the decay constant α_s and into the superlattice with the effective decay constant $\ln|\lambda|$, where λ can be expressed as

$$\lambda = \mathrm{e}^{-\alpha_1 l}\{\cosh(\alpha_2 h) - [(\beta_\mathrm{s}\beta_1 + \beta_2^2)/\beta_2(\beta_1 + \beta_\mathrm{s})]\sinh(\alpha_2 h)\}. \tag{6.7}$$

The normalisation of the shear modes discussed so far is an easy task, if the transfer matrix is used. For frequencies above the bulk threshold, i.e., in the continuous part of

the spectrum, the normalisation integral involves only the displacement field in the substrate [17], which is of the form

$$\boldsymbol{u}(\boldsymbol{x}) \sim \mathrm{e}^{\mathrm{i}\boldsymbol{Q}\cdot\boldsymbol{x}}\{\mathrm{e}^{\mathrm{i}q_z(z-ND)} + \mathrm{e}^{-\mathrm{i}[q_z(z-ND)+2\psi]}\} \tag{6.8}$$

where $q_z = |\alpha_s|$. The phase shift 2ψ, which results from the scattering of the shear bulk wave at the superlattice, can be calculated from the equation

$$\begin{pmatrix} 1 \\ -1 \end{pmatrix} \mathbf{R} \begin{pmatrix} \lambda^N & 0 \\ 0 & \lambda^{-N} \end{pmatrix} \mathbf{R}^{-1} \begin{pmatrix} \beta_1 \cos\psi + \mathrm{i}\beta_s \sin\psi \\ \beta_1 \cos\psi - \mathrm{i}\beta_s \sin\psi \end{pmatrix} = 0. \tag{6.9}$$

If the shear horizontal modes in the substrate continuum are normalised with respect to q_z, i.e.

$$\int_{-\infty}^{0} \mathrm{d}z\, \boldsymbol{w}^*(z|\boldsymbol{Q}q_z') \cdot \boldsymbol{w}(z|\boldsymbol{Q}q_z) = \delta(q_z' - q_z) \tag{6.10}$$

the spectral function in (3.10) gives rise to the density of state factor

$$\left|\frac{\mathrm{d}\alpha_s}{\mathrm{d}\Omega}\right| = \frac{\Omega}{c_s^2|\alpha_s|} \tag{6.11}$$

which becomes singular at the threshold frequency. This singularity is usually compensated by the matrix element, which is of the form

$$c_1(\beta_1 \cos\psi + \mathrm{i}\beta_s \sin\psi) + c_2(\beta_1 \cos\psi - \mathrm{i}\beta_s \sin\psi) \tag{6.12}$$

with regular coefficients c_1 and c_2. From (6.9), the phase ψ should behave as

$$\psi = \pm(\pi/2) + \mathrm{O}(\alpha_s) \tag{6.13}$$

unless the relation

$$\begin{pmatrix} 1 \\ -1 \end{pmatrix} \mathbf{R} \begin{pmatrix} \lambda^N & 0 \\ 0 & \lambda^{-N} \end{pmatrix} \mathbf{R}^{-1} \begin{pmatrix} 1 \\ 1 \end{pmatrix} = 0 \tag{6.14}$$

holds, which is the resonance condition for the 'plate modes' of the finite superlattice. If a solution of (6.14) comes close to the threshold frequency, we therefore expect a peak in the spectrum.

In figure 2, examples of the Brillouin spectra are given for three different values of N. The parameters used are listed in table 1. Since, to our knowledge, experimental data for the system considered here are not yet available, we have chosen the elastic parameters to be equal to those of Camley *et al* [5], to facilitate a comparison with their theoretical results. The dielectric constants and the ratio $p_{44}^{(1)}/p_{44}^{(2)}$ have been given arbitrary values in the range of those of semiconductors. The thermal quantum numbers in the spectral density function (3.12) are taken in the high-temperature limit. The discrete modes are indicated by vertical lines, the lengths of which measure their relative intensities. In the case of a substrate with a shear elastic constant lower than those of the films, no discrete shear horizontal modes exist, and only a continuous spectrum will be measured in the scattering geometry under consideration. Nevertheless, a fair amount of information can be extracted from the latter due to its remarkable oscillatory structure. With increasing N, the peaks of these oscillations close to the threshold frequency become sharper and higher. This can be understood on the basis of equations (6.9)–(6.11). For larger numbers of layers, the number of solutions of (6.9) increases, and

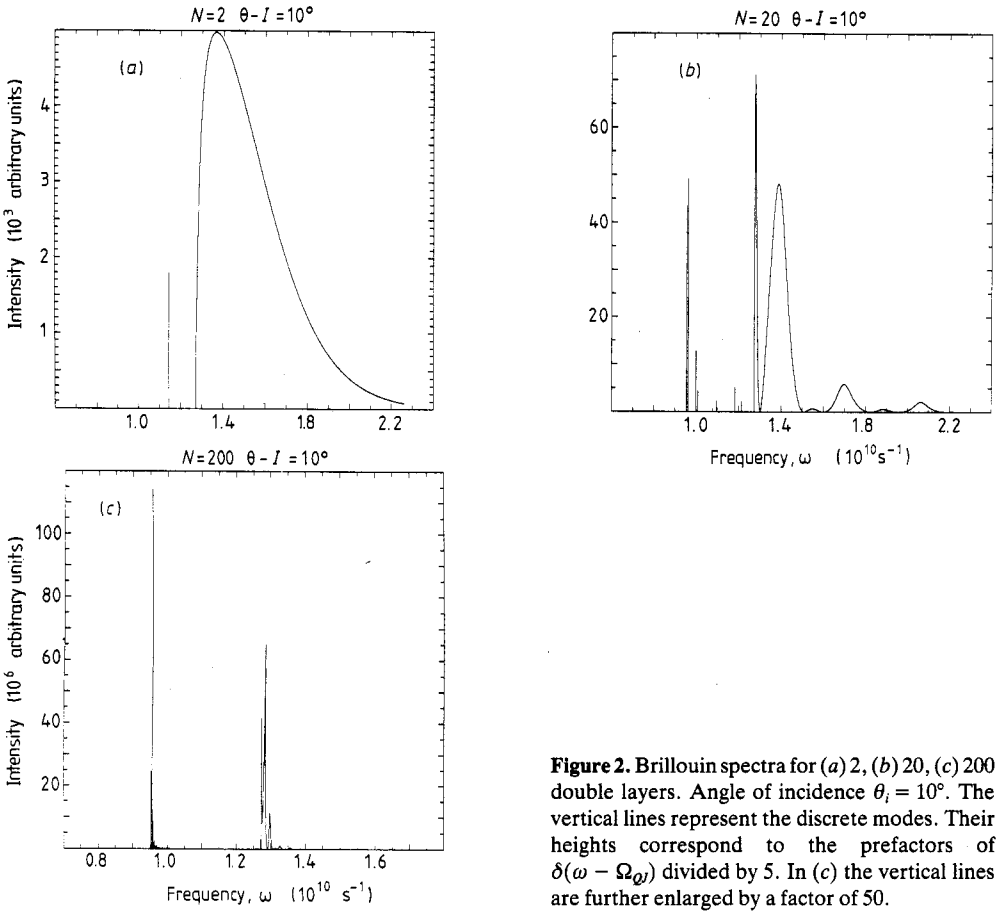

Figure 2. Brillouin spectra for (*a*) 2, (*b*) 20, (*c*) 200 double layers. Angle of incidence $\theta_i = 10°$. The vertical lines represent the discrete modes. Their heights correspond to the prefactors of $\delta(\omega - \Omega_{QJ})$ divided by 5. In (*c*) the vertical lines are further enlarged by a factor of 50.

Table 1. Parameters used for the numerical calculations. In all Brillouin spectra, the backscattering geometry has been considered.

	Layer type 1	Layer type 2	Substrate
Elastic parameters			
Shear velocities c_j [10^3 m s^{-1}]	1.83	2.905	3.0
Mass densities ρ_j (10^3 kg m^{-3}]	8.57	8.92	10.0
Thicknesses [10^{-7} m]	$\|l\| = 1.0$	$\|h\| = 0.5$	∞
Optical parameters			
Dielectric constants ε_j	15.0	10.0	
Pockels coefficients $p_{44}^{(j)}$	2.0	1.0	
Wavelength of incident light: $\lambda_0 = 5145 \times 10^{-10}$ m, $c_0 = 2.99 \times 10^8$ m.			

some of them may come close to the substrate threshold frequency thus giving rise to sharp peaks due to the small quantity $|\alpha_s|$ in the denominator.

Figure 3 shows a spectrum calculated with the same parameters as the previous two except for the angle of incidence (again, the backscattering geometry is considered).

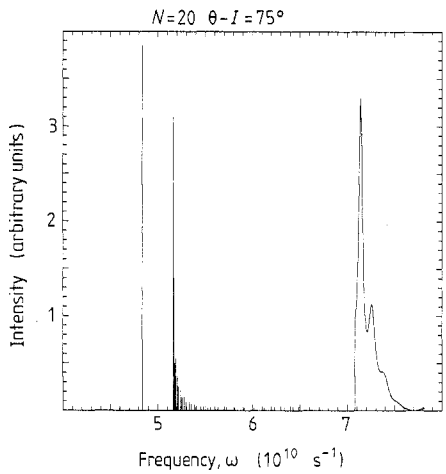

Figure 3. Brillouin spectrum for 20 double layers and angle of incidence $\theta_i = 75°$. The heights of the vertical lines correspond to the prefactors of $\delta(\omega - \Omega_{QJ})$ divided by 1000.

The number of discrete modes has strongly increased. Not all of the 43 modes can be seen in the figure, because the intensity decreases considerably as the threshold frequency of the substrate is approached. The situation in this case is distinct from that of the previous two figures in that both the incident and the scattered light fall into a forbidden optic band of the superlattice. This obviously influences the shape of the continuous spectrum. Now, the electromagnetic field consists of two parts, one of which decays exponentially from the vacuum side, the other from the substrate side into the superlattice. For sufficiently many layers, these two components are separated, and the scattering should resemble that of a metal, although both dielectric constants are real. For this peculiar case of total reflection, it is an easy task to calculate the Brillouin spectrum for a semi-infinite dielectric superlattice with our approach, as is demonstrated in § 7. In the case of propagating light in the superlattice, the limit $N \to \infty$ cannot be performed unambiguously, because the reference amplitudes, from which the amplitudes in the different layers are calculated via the transfer matrices, depend on N. If one has to deal with a semi-infinite superlattice, one rather has to require that, e.g., the modes of type a in § 5 are Bloch waves inside the medium propagating from the surface into the medium. This condition has been used for the incoming state by He *et al* [12] in their application of the matching method. The present approach can be extended to this case. For finite but very large N, the frequency separation of the elastic band modes can become smaller than the experimental resolution, so that a description of these modes as a continuous band is suggested, where the sum over the index J would be replaced by an integral. At this stage, the question arises, to what extent the density of states in these bands is affected by the boundary condition at the substrate interface. This problem requires a special investigation and is not pursued here.

7. Scattering from a semi-infinite superlattice with light of finite penetration depth

It has been pointed out by Yeh *et al* [16], that in dielectric superlattices the light propagates in the form of Bloch waves and there can be band gaps, i.e., for a given $\boldsymbol{K}$ and ω, the amplitudes decay exponentially with the distance from the surface. In figure

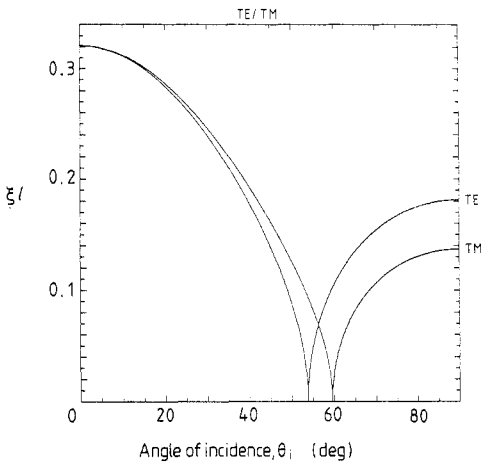

Figure 4. Effective wavevector component ξ in the z-direction for TE- and TM-polarised light as a function of the angle of incidence θ_i for the parameters in table 1. At a critical angle, ξ vanishes and for higher angles becomes imaginary.

4 the dependence of the effective wavevector component ξ and the inverse penetration depth on the angle of incidence is shown for the parameters chosen in our numerical examples for both types of polarisation. The penetration depth always extends over at least several units of the superlattice. The normal modes of the electromagnetic field in this particular regime of $\boldsymbol{K}$ and ω, where the effective wavevector component in the z-direction is imaginary, are easily determined. They are of type a and the two-component amplitude vectors in the layers of type 1 are proportional to the eigenvector of the transfer matrix associated with the larger eigenvalue. In figure 5, an example of a Brillouin spectrum is shown for this case. The parameters used are again those of table 1 and the parallel component of the wavevector is $|Ql| = 2.359$. For comparison, the spectral density $S(\boldsymbol{Q}, \omega, z)$ introduced by Camley *et al* [5] is also displayed for $z = 0$, where it can be written as

$$S(\boldsymbol{Q}, \omega, z = 0) \sim |A_{1\pm}^{(0)}|^2 \omega^{-2} \delta(\omega - \Omega_{QJ}) \tag{7.1a}$$

for the discrete modes,

$$S(Q, \omega, z = 0) \sim |A_{1\pm}^{(0)}|^2 \, \omega^{-2} \left| \frac{\mathrm{d}\zeta}{\mathrm{d}\Omega} \right| \tag{7.1b}$$

in the continuous regions. The amplitudes $A_{1+}^{(0)} = A_{1-}^{(0)}$ in the uppermost layer are determined by the normalisation. The continuous modes are conveniently normalised with respect to the effective wavenumber ζ, which gives rise to the density of states factor in (7.1*b*). A remarkable difference between the spectral density at the surface and the Brillouin spectrum consists in the much steeper fall-off of the latter with increasing frequency. Furthermore, certain gap modes are not visible in the Brillouin spectrum. It seems to be difficult to explain this behaviour by simple arguments.

Since the slope of the dispersion curve of the band modes as function of ζ usually vanishes at the Brillouin zone boundary, the density of state factor entering the spectral density as well as the scattering intensity has a singularity. This is, however, compensated by the normalisation of the elastic modes in a subtle way, which has its mathematical origin in the fact that at the zone boundary the transfer matrix has the single eigenvalue

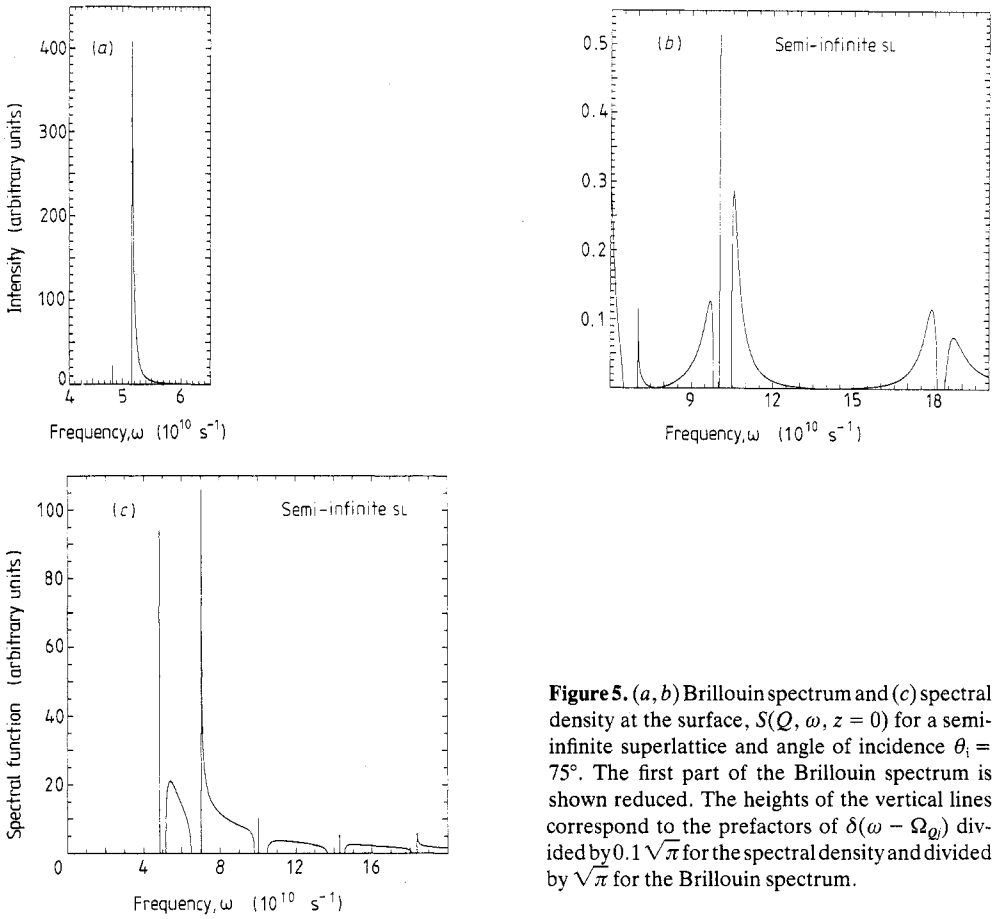

Figure 5. (a, b) Brillouin spectrum and (c) spectral density at the surface, $S(Q, \omega, z = 0)$ for a semi-infinite superlattice and angle of incidence $\theta_i = 75°$. The first part of the Brillouin spectrum is shown reduced. The heights of the vertical lines correspond to the prefactors of $\delta(\omega - \Omega_{Q_i})$ divided by $0.1\sqrt{\pi}$ for the spectral density and divided by $\sqrt{\pi}$ for the Brillouin spectrum.

1, which is not degenerate, if the off-diagonal element T_{12} does not vanish. If the latter occurs, i.e., if

$$\beta_1^2 = \beta_2^2 \tag{7.2}$$

or

$$\exp(2\alpha_2 h) = 1 \tag{7.3}$$

the density of state factor is no longer singular and crossings of band edges may take place. Such crossings have been found [5] and correspond to condition (7.2), i.e., they are situated in the Ω–Q plane at the intersections between the band edges and the straight line given by the equation

$$\frac{\omega}{Q} = \left(\frac{\rho_1^2 c_1^4 - \rho_2^2 c_2^4}{\rho_1^2 c_1^2 - \rho_2^2 c_2^2}\right)^{1/2}. \tag{7.4}$$

8. Conclusions

The theory of Brillouin scattering from layered dielectric elastic media has been formulated in the framework of the distorted-wave Born approximation. The resulting

general formula for the intensity of the scattered light has been applied to example systems, for which its evaluation seems to be particularly easy, namely to crossed polarised scattering of a finite dielectric superlattice on a totally reflecting substrate and of a semi-infinite dielectric superlattice under the condition of a finite penetration depth of the light. In this geometry, the shear horizontal elastic modes in the superlattices can be studied. Brillouin scattering experiments on these systems for various angles of incidence would be desirable to investigate their interesting spectral properties and enable a comparison with the present theory.

Acknowledgments

The author benefited from stimulating discussions with Professors V Bortolani, F Nizzoli, G Santoro and R K Wehner, and would like to thank Professor A A Maradudin for helpful comments and a critical reading of the manuscript. He also gratefully acknowledges the hospitality of the Physics Departments of the University of California, Irvine and the University of Perugia and financial support from the Deutsche Forschungsgemeinschaft.

Appendix

The transfer matrices used in the calculations of § 6 are of the general form

$$\mathbf{T} = \frac{1}{4b_1b_2} \times \begin{bmatrix} [(b_1+b_2)^2 e^{-a_2h} - (b_1-b_2)^2 e^{a_2h}]e^{-a_1l} & (e^{a_2h} - e^{-a_2h})(b_1^2 - b_2^2)e^{-a_1l} \\ (e^{-a_2h} - e^{a_2h})(b_1^2 - b_2^2)e^{a_1l} & [(b_1+b_2)^2 e^{a_2h} - (b_1-b_2)^2 e^{-a_2h}]e^{a_1l} \end{bmatrix} \tag{A1}$$

and the matrices **M** introduced in § 5 are given by

$$\mathbf{M} = \frac{1}{2b_1'} \begin{bmatrix} (b_1+b_2)e^{(a_2-a_1)l} & (b_1-b_2)e^{-(a_1+a_2)l} \\ (b_1-b_2)e^{(a_1+a_2)l} & (b_1+b_2)e^{(a_1-a_2)l} \end{bmatrix}. \tag{A2}$$

The following identifications have to be made:

$$a_j = iq_{0j} \qquad b_j = q_{0j} \qquad j = 1, 2 \qquad b_1' = b_1 \tag{A3}$$

for the incoming TE modes,

$$a_j = iq_j \qquad j = 1, 2 \qquad b_1 = \varepsilon_2 q_1 \qquad b_2 = \varepsilon_1 q_2 \qquad b_1' = (\varepsilon_1/\varepsilon_2)b_1 \tag{A4}$$

for the outgoing TM modes,

$$a_j = \alpha_j \qquad b_j = \beta_j \qquad j = 1,2 \qquad b_1' = b_1 \tag{A5}$$

for the elastic shear horizontal modes. The function F in the matrix element can be decomposed as follows

$$\begin{aligned} F_{\sigma_1\sigma_2\sigma_3}(\boldsymbol{kk}_0|ss_0|JN) = \sum_{\sigma_1'\sigma_2'\sigma_3'=\pm} & \{m_1(\sigma_1'\sigma_2'\sigma_3')R_{\sigma_1'\sigma_1}(\boldsymbol{QJ})R^*_{\sigma_2'\sigma_2}(\boldsymbol{ks}) \\ & \times R_{\sigma_3'\sigma_3}(\boldsymbol{k}_0 s_0) + m_2(\sigma_1'\sigma_2'\sigma_3')[\mathbf{M}^{-1}(\boldsymbol{QJ})\mathbf{R}(\boldsymbol{QJ})]_{\sigma_1'\sigma_1} \\ & \times [\mathbf{M}^{-1}(\boldsymbol{ks})\mathbf{R}(\boldsymbol{ks})]^*_{\sigma_2'\sigma_2}[\mathbf{M}^{-1}(\boldsymbol{k}_0 s_0)\mathbf{R}(\boldsymbol{k}_0 s_0)]_{\sigma_3'\sigma_3}\} \\ & \times t_{\sigma_1}(\boldsymbol{QJ})t^*_{\sigma_2}(\boldsymbol{ks})t_{\sigma_3}(\boldsymbol{k}_0 s_0)A^{(N-1)*}_{2+}(\boldsymbol{ks}) \\ & \times A^{(N-1)}_{2+}(\boldsymbol{k}_0 s_0)A_{s+}(\boldsymbol{QJ}) \end{aligned} \tag{A6}$$

where

$$m_1(\sigma_1\sigma_2\sigma_3) = f_1(\sigma_1\sigma_2)\frac{1-\exp[(\sigma_1\alpha_1 - \mathrm{i}\sigma_2 q_1 + \mathrm{i}\sigma_3 q_{01})l]}{\sigma_1\alpha_1 - \mathrm{i}\sigma_2 q_1 + \mathrm{i}\sigma_3 q_{01}} \tag{A7a}$$

$$\begin{aligned} m_2(\sigma_1\sigma_2\sigma_3) = {} & f_2(\sigma_1\sigma_2) \\ & \times \frac{\exp[(\sigma_1\alpha_1 - \mathrm{i}\sigma_2 q_2 + \mathrm{i}\sigma_3 q_{02})l] - \exp[(\sigma_1\alpha_1 - \mathrm{i}\sigma_2 q_2 + i\sigma_3 q_{02})D]}{\sigma_1\alpha_2 - \mathrm{i}\sigma_2 q_2 + \mathrm{i}\sigma_3 q_{02}} \end{aligned} \tag{A7b}$$

and

$$\begin{aligned} f_j(\sigma_1\sigma_2) = {} & \left(\frac{\hbar^3}{32(\omega-\omega_0)(1+q_0^2/K^2)}\right)^{1/2} \omega\varepsilon_f^2 p_{44}^{(j)} \\ & \times [-\mathrm{i}(K-K_0)\sigma_2(q_j/K) + \sigma_1\alpha_j]. \end{aligned} \tag{A8}$$

The amplitudes of the shear modes are defined analogously to (5.1) with $\mathrm{i}q_j$ replaced by α_j. The two-component vectors t are determined by the boundary conditions at the substrate interface and the reference amplitudes by the normalisation. For the incoming TE mode, we obtain

$$t = \mathbf{R}^{-1}\begin{pmatrix}1\\-1\end{pmatrix}\frac{q_{02}}{q_{01}}\mathrm{e}^{\mathrm{i}q_{02}D} \tag{A9}$$

$$\begin{aligned} A^{(N-1)}_{2+} = {} & 2q_{00}\{\lambda^N t_+[q_{00}(R_{11}+R_{21}) + q_{01}(R_{11}-R_{21})] \\ & + \lambda^{-N}t_-[q_{00}(R_{12}+R_{22}) + q_{01}(R_{12}-R_{22})]\}^{-1}A_{v+} \end{aligned} \tag{A10}$$

and for the outgoing TM mode

$$t = R^{-1}\begin{pmatrix}1\\1\end{pmatrix}\frac{\varepsilon_2}{\varepsilon_1}\mathrm{e}^{\mathrm{i}q_2 D} \tag{A11}$$

$$\begin{aligned} A^{(N-1)}_{2+} = {} & 2q_0\{\lambda^N t_+[\varepsilon_1 q_0(R_{11}+R_{21}) + q_1(R_{11}-R_{21})] \\ & + \lambda^{-N}t_-[\varepsilon_1 q_0(R_{12}+R_{22}) + q_1(R_{12}-R_{22})]\}^{-1}A_{v+}. \end{aligned} \tag{A12}$$

For the elastic modes below the substrate bulk threshold, we have

$$t = \frac{1}{2\beta_1}\mathbf{R}^{-1}\begin{pmatrix}\beta_1 + \beta_s\\ \beta_1 - \beta_s\end{pmatrix} \tag{A13}$$

and for the elastic modes in the continuous spectrum

$$t = \frac{1}{\beta_1}\mathbf{R}^{-1}\begin{pmatrix}\beta_1\cos\psi + \mathrm{i}\beta_s\sin\psi\\ \beta_1\cos\psi - \mathrm{i}\beta_s\sin\psi\end{pmatrix}. \tag{A14}$$

References

[1] Sandercock J R 1970 *Opt. Commun.* **2** 73
[2] Subbaswamy K R and Maradudin A A 1978 *Phys. Rev.* B **18** 4181
[3] Marvin A, Bortolani V and Nizzoli F 1980 *J. Phys. C: Solid State Phys.* **13** 299
[4] Bortolani V and Levi A C 1986 *Rivista del Nuovo Cimento* **9** (11)
[5] Camley R E, Djafari-Rouhani B, Dobrzynski L and Maradudin A A 1983 *Phys. Rev.* B **27** 7318
[6] Djafari-Rouhani B, Dobrzynski L, Hardouin Duparc O, Camley R E and Maradudin A A 1983 *Phys. Rev.* B **28** 1711
[7] Babiker M, Tilley D R, Albuquerque E L and Goncalves da Silva C E T 1985 *J. Phys. C: Solid State Phys.* **18** 1269
[8] Babiker M, Tilley D R and Albuquerque E L 1985 *J. Phys. C: Solid State Phys.* **18** 1285
[9] Baumgart P, Hillebrands B, Mock R, Guntherodt G, Boufelfel A and Falco C M 1986 *Phys. Rev.* B **34** 9004
[10] Bell J A, Bennett W R, Zanoni R, Stegeman G I, Falco C M and Nizzoli F 1987 *Phys. Rev.* B **35** 4127
[11] Sapriel J, Chavignon J, Alexandre F and Azoulay R 1986 *Phys. Rev.* B **34** 7118
[12] He J, Djafari-Rouhani B and Sapriel J 1988 *Phys. Rev.* B **37** 4086
[13] Sapriel J, He J, Djafari-Rouhani B, Azoulay R and Mollot F 1988 *Phys. Rev.* B **37** 4099
[14] Taylor J R 1972 *Scattering Theory* (New York: Wiley)
[15] Mills D L, Maradudin A A and Burstein E 1970 *Ann. Phys.* **56** 504
[16] Yeh P, Yariv A and Hong C S 1977 *J. Opt. Soc. Am.* **67** 423
[17] Bortolani V, Marvin A M, Nizzoli F and Santoro G 1983 *J. Phys. C: Solid State Phys.* **16** 1757